BIOCHEMISTRY
including biophysical chemistry & molecular biology

Article

pubs.acs.org/biochemistry

Fourier Transform Infrared Detection of a Polarizable Proton Trapped between Photooxidized Tyrosine Y_Z and a Coupled Histidine in Photosystem II: Relevance to the Proton Transfer Mechanism of Water Oxidation

Shin Nakamura, Ryo Nagao, Ryouta Takahashi, and Takumi Noguchi*

Division of Material Science, Graduate School of Science, Nagoya University, Furo-cho, Chikusa-ku, Nagoya 464-8602, Japan

Supporting Information

ABSTRACT: The redox-active tyrosine Y_Z (D1-Tyr161) in photosystem II (PSII) functions as an immediate electron acceptor of the Mn_4Ca cluster, which is the catalytic center of photosynthetic water oxidation. Y_Z is also located in the hydrogen bond network that connects the Mn_4Ca cluster to the lumen and hence is possibly related to the proton transfer process during water oxidation. To understand the role of Y_Z in the water oxidation mechanism, we have studied the hydrogen bonding interactions of Y_Z and its photooxidized neutral radical $Y_Z^\bullet$ together with the interaction of the coupled His residue, D1-His190, using light-induced Fourier transform infrared (FTIR) difference spectroscopy. The $Y_Z^\bullet$-minus-Y_Z FTIR difference spectrum of Mn-depleted PSII core complexes exhibited a broad positive feature around 2800 cm^{-1}, which was absent in the corresponding spectrum of another redox-active tyrosine Y_D (D2-Tyr160). Analyses by ^{15}N and H/D substitutions, examination of the pH dependence, and density functional theory and quantum mechanics/molecular mechanics (QM/MM) calculations showed that this band arises from the N−H stretching vibration of the protonated cation of D1-His190 forming a charge-assisted strong hydrogen bond with $Y_Z^\bullet$. This result provides strong evidence that the proton released from Y_Z upon its oxidation is trapped in D1-His190 and a positive charge remains on this His. The broad feature of the ∼2800 cm^{-1} band reflects a large proton polarizability in the hydrogen bond between $Y_Z^\bullet$ and $HisH^+$. QM/MM calculations further showed that upon Y_Z oxidation the hydrogen bond network is rearranged and one water molecule moves toward D1-His190. From these data, a novel proton transfer mechanism via $Y_Z^\bullet$-$HisH^+$ is proposed, in which hopping of the polarizable proton of $HisH^+$ to this water triggers the transfer of the proton from substrate water to the luminal side. This proton transfer mechanism could be functional in the $S_2 \rightarrow S_3$ transition, which requires proton release before electron transfer because of an excess positive charge on the Mn_4Ca cluster.

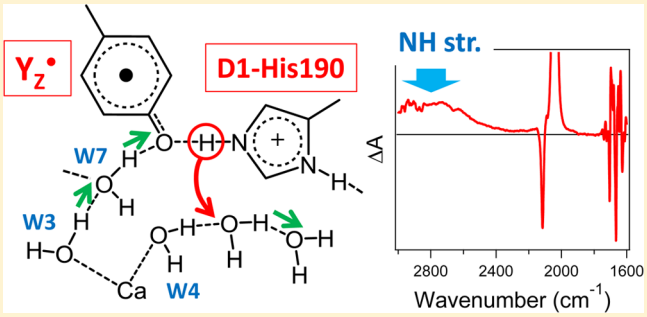

In oxygenic photosynthesis performed by plants and cyanobacteria, water is utilized as the ultimate source of electrons that are used for reduction of carbon dioxide to produce sugars. Oxidation of water, which results in the release of molecular oxygen and protons, is performed in photosystem II (PSII) protein complexes embedded in thylakoid membranes.[1−7] In PSII, light-induced charge separation takes place at the excited state of the reaction center chlorophylls (the coupled state of Chl_{D1} and chlorophyll dimer P680) to eject an electron to the pheophytin (Pheo) electron acceptor, resulting in a charge-separated state, $P680^+Pheo^-$.[8,9] The electron is subsequently transferred to the primary quinone electron acceptor Q_A, and then the secondary quinone acceptor Q_B. On the electron donor side, $P680^+$ first oxidizes the redox-active tyrosine Y_Z (D1-Tyr161) and then Y_Z oxidizes the Mn_4Ca cluster, where water is oxidized via a light-driven cycle of five intermediates called S_i states (i = 0−4).[1−7]

When Y_Z is oxidized by $P680^+$, the phenolic proton is released because of the extremely low pK_a (approximately −2)[10] of the radical cation of a phenolic group, forming a neutral $Y_Z^\bullet$ radical.[11−13] The X-ray structure of PSII revealed that the phenolic oxygen of Y_Z is within hydrogen bonding distance of the neighboring D1-His190 (Figure 1A).[14−16] In particular, the recent high-resolution (1.9 Å) X-ray structure exhibited a significantly short distance of 2.46 Å between the Y_Z oxygen and the N_τ atom of D1-His190,[16] which was reproduced by the quantum mechanics/molecular mechanics (QM/MM) calculation, showing the presence of a strong hydrogen bond with a single well potential.[17] Upon oxidation, the proton of Y_Z is thought to shift to N_τ of D1-His190 along this strong hydrogen bond, which is the basic mechanism of the fast proton-coupled electron transfer (PCET) of Y_Z.[11−13,17,18] Whether the positive charge remains on this His residue during the lifetime of $Y_Z^\bullet$ has been a matter of debate.[12,19−22] Even if

Received: February 24, 2014
Revised: April 22, 2014
Published: April 30, 2014

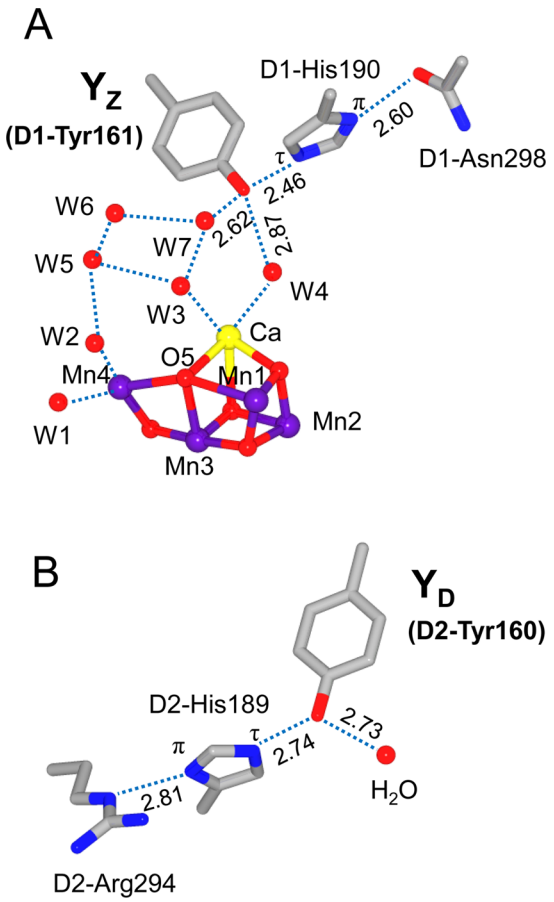

Figure 1. Structures of the hydrogen bond networks around Y_Z (A) and Y_D (B) deduced from the X-ray crystallographic structure of photosystem II at 1.9 Å resolution (PDB entry 3ARC[16]).

the proton of N_τ-H is not released, the proton at N_π, the other nitrogen of the imidazole, could be released in a protein relaxation phase in the microsecond time regime after the fast nanosecond phase of electron transfer.[5,13] Although several lines of data supported the presence of a positive charge near $Y_Z^\bullet$,[12,22−24] further direct evidence is necessary to reach the final conclusion.

The high-resolution X-ray structure[16] also showed that Y_Z interacts with the Mn_4Ca cluster via a water cluster that consists of several water molecules (Figure 1A). Water W4 (the nomenclature of the water molecules and Mn atoms follows that of Umena et al.[16]) directly connects the Y_Z oxygen and the Ca atom, while W3, another water ligand to Ca, interacts with Y_Z thorough W7. W2, the water ligand to Mn4, also interacts with Y_Z through the water molecules, W5, W6, W3, and W7. The X-ray structure further showed that Y_Z is located in a hydrogen bond network connecting the Mn_4Ca cluster to the lumen, which has been suggested to be one of the proton exit or water access pathways.[16,25−27] It is thus possible that Y_Z functions as a proton transfer mediator in this pathway during water oxidation.

Another redox-active tyrosine Y_D (D2-Tyr160) in PSII (Figure 1B), which is symmetrically related to Y_Z, also donates an electron to $P680^+$. The structure of the Y_D site is very similar to that of Y_Z. The phenolic oxygen of Y_D is within hydrogen bonding distance of D2-His189 and a water molecule (Figure 1B). However, the rate of oxidation of Y_D is much slower than that of Y_Z, and the resultant $Y_D^\bullet$ radical is considerably stable at room temperature.[11,12] Thus, Y_D functions only as a peripheral electron donor to $P680^+$ and is not directly related to water oxidation. The lower redox potential of Y_D (700−800 mV)[28,29] compared with that of Y_Z (900−1000 mV)[29,30] and the proton release mechanism involving a mobile water[31] have been suggested as causes for its radical stability and the slow kinetics of the redox reaction.

One of the major questions relevant to Y_Z function is its role in the water oxidation mechanism.[12,13,19,32,33] Does Y_Z function only as an electron mediator between P680 and the Mn_4Ca cluster, or is it more deeply involved in the proton release processes during water oxidation? If the latter is the case, what is the mechanism of the PCET involving Y_Z and the Mn_4Ca cluster, and does the proton pathway involving Y_Z actually function in some of the S-state transitions? With this respect, it is important to answer the question of whether a proton is released from D1-His190 upon Y_Z oxidation or a positive charge is trapped on this His throughout the lifetime of $Y_Z^\bullet$? If the proton is released into the bulk, $Y_Z^\bullet$ can abstract a proton of substrate water through the hydrogen bond network concomitant with electron transfer, as was previously proposed as a hydrogen abstraction model by Babcock and co-workers.[19] In addition, it has been argued that a positive charge near $Y_Z^\bullet$ triggers the release of the proton from substrate water by electrostatic interaction with the Mn_4Ca cluster.[32−36] It is also crucial to obtain the information about the protonation structures and hydrogen bonding interactions of Y_Z and the coupled His to argue the possibility of transfer of the proton through Y_Z for releasing a proton from the Mn_4Ca center.

In this study, we have investigated the hydrogen-bonded structure of the Y_Z-His moiety and its change upon photooxidation using light-induced Fourier transform infrared (FTIR) difference spectroscopy. FTIR difference spectroscopy has been extensively used for the investigation of the water oxidation mechanism and various redox reactions in photosystem II.[37−43] The $Y_Z^\bullet$-minus-Y_Z FTIR difference spectrum (hereafter designated the $Y_Z^\bullet/Y_Z$ difference spectrum) in the 1800−1000 cm^{-1} region was previously reported by Berthomieu et al.[44] Here, we have obtained $Y_Z^\bullet/Y_Z$ spectra that include the higher-frequency region that involves the vibrations of protons. The spectra were analyzed by isotopic substitutions and pH changes, and also by comparison with a $Y_D^\bullet/Y_D$ difference spectrum. Furthermore, we have performed quantum chemical calculations using density functional theory (DFT) and QM/MM methods for the Y_Z-His and Y_D-His pairs to interpret the experimental spectra and obtain structural information. The proton trapped between Y_Z and D1-His190 upon its photooxidation was directly detected as a broad N-H stretching band of the His, revealing a large proton polarizability. Information about the protonation and hydrogen-bonded structures of Y_Z and D1-His190 and the nearby hydrogen bond network was also obtained. On the basis of the results, the roles of Y_Z and the coupled His in the PCET mechanism of water oxidation are discussed.

MATERIALS AND METHODS

Preparation of PSII Core Complexes. The thermophilic cyanobacterium *Thermosynechococcus elongates* 47-H strain, in which a six-histidine tag was introduced onto the C-terminus of the CP47 subunit, was grown in a BG11 medium[45] supplemented with 10 mM Hepes (pH 7.5) by stirring and bubbling with air containing 3% (v/v) CO_2.[46] Global ^{15}N substitution was performed by culturing cells in a BG11

dx.doi.org/10.1021/bi500237y | *Biochemistry* 2014, 53, 3131−3144

medium containing $Na^{15}NO_3$ (SI Science Co., Ltd.; 99.7 atom % ^{15}N) and $CoCl_2$ instead of unlabeled $NaNO_3$ and $Co(NO_3)_2$, respectively.

Oxygen-evolving PSII complexes were purified using the method by Boussac et al.[47] with some modifications. Cells were washed once with a 40 mM sodium phosphate buffer (pH 7.0) containing 1 mM EDTA and then suspended in a buffer containing 40 mM Mes (pH 6.5), 10 mM $CaCl_2$, 10 mM $MgCl_2$, 10% (w/v) glycerol, and 1 M betaine (buffer A). The cells were disrupted in buffer A in the presence of 0.2% (w/v) bovine serum albumin, 1 mM benzamidine, 1 mM amino-caproic acid, and 50 μg/mL DNase I by agitation with glass beads (100 μm in diameter), repeating the on (10 s) and off (3 min) cycle 19 times on ice in the dark. The lysate was diluted with an equal volume of a buffer containing 40 mM Mes-NaOH (pH 6.5), 10 mM $CaCl_2$, and 10 mM $MgCl_2$. Unbroken cells were removed by centrifugation at 3000*g* for 5 min, and the supernatant was subsequently centrifuged at 48000*g* for 20 min. Obtained thylakoid membranes suspended in buffer A were solubilized with 1% (w/v) *n*-dodecyl β-D-maltoside (DM) at a chlorophyll (Chl) concentration of 1.0 mg/mL while being gently stirred for 10 min on ice in the dark. After centrifugation at 48000*g* for 10 min, the resultant supernatant was applied to a Ni^{2+} affinity column equilibrated with buffer A containing 20 mM imidazole, 100 mM NaCl, and 0.03% DM. PSII complexes were eluted with buffer A containing 200 mM imidazole, 100 mM NaCl, and 0.03% DM and then washed with buffer A containing 0.03% DM by ultrafiltration (Vivaspin 20, Sartorium Stedim, 100 kDa molecular mass cutoff). The O_2 evolution activity of the obtained PSII core complexes with 0.5 mM 2,6-dichloro-1,4-benzoquinone as an electron acceptor was 2400−2700 μmol of O_2 (mg of Chl)$^{-1}$ h^{-1}. Mn depletion was performed via a 10 mM NH_2OH treatment for 30 min at room temperature, followed by a wash with buffer A containing 0.03% DM by ultrafiltration (Vivaspin 20).

FTIR Measurements. For $Y_Z^{\bullet}/Y_Z$ FTIR measurements, Mn-depleted PSII core complexes were suspended in a buffer that consisted of 20 mM Mes (pH 6.5 or 5.5) or 20 mM Hepes (pH 7.5) containing 40 mM sucrose, 10 mM NaCl, 5 mM $MgCl_2$, and 0.06% DM and concentrated to ∼6 mg/mL Chl by ultrafiltration (Vivaspin 500, 100 kDa molecular mass cutoff). Four microliters of the suspension was mixed with 1 μL of 100 mM potassium ferricyanide and then dried on a BaF_2 plate (13 mm in diameter) under a N_2 gas flow. The sample was sandwiched with another BaF_2 plate with 0.8 μL of H_2O. For the preparation of samples in D_2O, the dried core complexes were resuspended in 3 μL of D_2O and dried again. This process was repeated several times, and finally, the sample was sandwiched with 0.8 μL of D_2O. The sample temperature was adjusted to 250 K in a cryostat (Oxford DN1704).

Flash-induced FTIR spectra were recorded on a Bruker IFS-66/S spectrophotometer equipped with an MCT detector (D313-L). Flash illumination was performed using a Q-switched Nd:YAG laser (INDI-40-10; 532 nm; ∼7 ns full width at half-maximum; ∼7 mJ pulse^{-1} cm^{-2}). For $Y_Z^{\bullet}/Y_Z$ spectra, single-beam spectra with 50 scans (25 s accumulation) were recorded twice before and once after single-flash illumination. The measurement was repeated with a dark interval of 225 s between measurements (flash illumination every 5 min). The spectra of 350−1000 loops recorded using one to four samples were averaged to calculate a light-minus-dark difference spectrum as a $Y_Z^{\bullet}/Y_Z$ difference spectrum and a dark-minus-dark difference spectrum before illumination representing the baseline and noise level.

The $Y_D^{\bullet}/Y_D$ FTIR spectrum was measured with the method described previously[48] with some modification. Briefly, 5 μL of a suspension of the Mn-depleted PSII complexes (3 mg/mL Chl) in a pH 6.5 Mes buffer (10 mM Mes, 5 mM NaCl, and 0.06% DM) was mixed with 1 μL of 20 mM potassium ferricyanide and 1 μL of 20 mM potassium ferrocyanide. The sample was dried on a BaF_2 plate to make a film and then sealed with another BaF_2 plate with 2 μL of a 40% (v/v) glycerol/H_2O mixture without touching the sample. H/D exchange was performed by repeating drying and resuspension in D_2O, which was similar to the process used for samples for Y_Z measurements. The sample temperature was adjusted to 283 K by circulating cold water in a copper holder. Single-beam spectra with 100 scans (50 s accumulation) were recorded twice before and once after five flashes (1 Hz) from the Nd:YAG laser, and the measurement was repeated with a dark interval of 750 s. The spectra of 54 loops were averaged to calculate a light-minus-dark difference spectrum as a $Y_D^{\bullet}/Y_D$ spectrum and a dark-minus-dark difference spectrum as the baseline.

Quantum Chemical Calculations. Quantum chemical calculations were performed using the Gaussian09 program package.[49] For DFT calculations for the Tyr-His models, the B3LYP functional[50,51] with the 6-31++G(d,p) basis set was used to optimize the geometries and calculate the vibrational frequencies and IR intensities. QM/MM calculations were performed using the ONIOM (our own *n*-layered integrated molecular orbital and molecular mechanics) method.[52] For Y_Z calculations, the atomic coordinates of amino acid residues, water molecules, the Mn_4CaO_5 cluster, and Cl^- ions located within 20 Å of the Ca atom were taken from the X-ray structure of the PSII complexes at 1.9 Å resolution (PDB entry 3ARC[16]). The hydrogen atoms were generated and optimized using Amber. The geometry of the Mn_4CaO_5 cluster and surrounding groups (Cl^- ions, amino acid ligands to Mn, Ca, and Cl^-, Y_Z, D1-His190, D1-Asp61, W1−W7, HOH446, and HOH442) was then optimized as a QM region fixing other atoms as a MM region. In this optimization, we used the model of the Mn_4CaO_5 cluster with (Mn1, Mn2, Mn3, Mn4) = (III, IV, IV, III), W2 = H_2O, and O5 = O^{2-}.[53] Using the obtained coordinates and atomic partial charges, further geometry optimization and vibrational analysis were performed for Y_Z and the surrounding groups (D1-His190, D1-Asn298, D1-Gln165, Ca, W3−W7, HOH387, HOH394, HOH398, HOH778, HOH923, and HOH1117) as a QM region (Figure S2 of the Supporting Information), fixing the other atoms in the MM region using ONIOM (B3LYP:Amber). As basis sets in the QM calculation, LANL2DZ is used for Ca and Mn and 6-31++G(d,p) for other atoms. For Y_D calculation, the atomic coordinates of amino acid residues and water molecules located within 20 Å of Y_D were taken from the X-ray structure (PDB entry 3ARC[16]), and then the hydrogen atoms were generated and optimized using Amber. Geometry optimization and vibrational analysis were performed for Y_D and the surrounding groups (D2-His189, D2-Arg294, D2-Arg180, and HOH1) as a QM region (Figure S3 of the Supporting Information), fixing the other atoms in the MM region using ONIOM [B3LYP/6-31++G(d,p):Amber].

Calculated vibrational frequencies by the DFT and ONIOM methods were scaled to adjust the CO frequencies of the $Y_Z^{\bullet}$ and $Y_D^{\bullet}$ radicals to the experimental frequencies, 1514 and 1504 cm^{-1}, respectively. The scaling factors for the Y_Z-His and

dx.doi.org/10.1021/bi500237y | *Biochemistry* 2014, 53, 3131−3144

Y_D-His pairs were 0.979 and 0.987, respectively, in the DFT calculations and 0.968 and 0.973, respectively, in the ONIOM calculations. The calculated frequencies of free 4-methylimidazole (4-MeIm) were scaled by a factor of 0.980 following the previous DFT calculation of the various protonation forms of 4-MeIm.[54]

RESULTS

An FTIR difference spectrum (3000−1000 cm^{-1}) of Y_Z upon its photooxidation ($Y_Z^{\bullet}/Y_Z$ spectrum), which was measured using the Mn-depleted PSII core complexes from *Thermosynechococcus elongatus* at pH 6.5, is shown in Figure 2 (solid line)

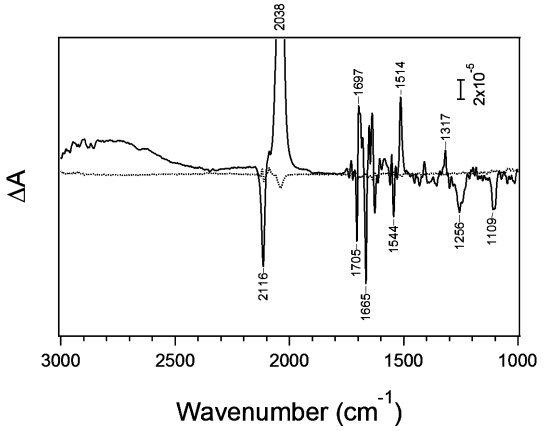

Figure 2. Light-induced $Y_Z^{\bullet}/Y_Z$ FTIR difference spectrum (3000−1000 cm^{-1}) of the PSII core complexes from *T. elongatus* (—) together with a dark-minus-dark spectrum representing a baseline (···).

together with a dark/dark spectrum (dotted line) representing a baseline. The large peaks at 2116 and 2038 cm^{-1} arise from the CN stretching vibrations of ferricyanide and ferrocyanide, respectively, reflecting the flow of an electron from the electron donor side to the acceptor side. Note that small peaks at the same positions in opposite signs in the dark/dark spectrum are due to the residual back reaction (~4% of the forward reaction) during the measurements of the two dark spectra before illumination (see Materials and Methods). The $Y_Z^{\bullet}/Y_Z$ spectrum in the 1800−1000 cm^{-1} region (expanded in Figure 3a) is very similar to the spectrum previously reported by Berthomieu et al.[44] using the Mn-depleted preparations of the PSII core complexes from *Synechocystis* sp. PCC 6803 and PSII-enriched membranes from spinach. The positive band at 1514 cm^{-1} arises from the CO stretching (ν_{CO}) vibration of the oxidized $Y_Z^{\bullet}$ radical,[39,44] while the corresponding band of $Y_D^{\bullet}$ was observed at 1504 cm^{-1} (Figure 3d).[48,55] Berthomieu et al.[44] previously assigned a negative band at 1255 cm^{-1} in their $Y_Z^{\bullet}/Y_Z$ spectrum to the COH bending (δ_{COH}) vibration of reduced Y_Z and a small negative peak at 1279 cm^{-1} to its ν_{CO} vibration. We did not observe the latter peak and prefer the assignment of the relatively broad band at 1256 cm^{-1} (Figure 3a) to the overlap of the δ_{COH} and ν_{CO} vibrations, which are more or less coupled with each other.[56,57] Indeed, in D_2O (Figure 3c), a narrower band was left at an upshifted position of 1262 cm^{-1}, which is assigned to the pure ν_{CO} vibration decoupled from the δ_{COH} vibration.[57] The differential signal at 1705/1697 cm^{-1} was temporally assigned to the electrochromic shift of the keto CO band of P680 by Y_Z oxidation,[44] while most of the other bands in the 1700−1600 cm^{-1} region probably arise from the amide I vibrations (CO stretches) of backbone amides due to the

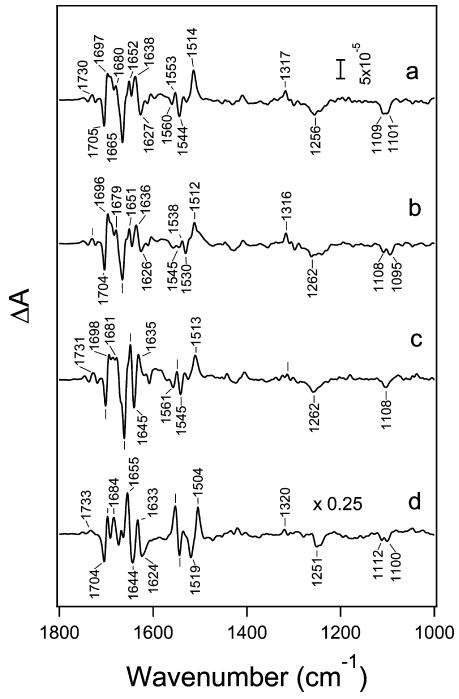

Figure 3. $Y_Z^{\bullet}/Y_Z$ FTIR difference spectra (1800−1000 cm^{-1}) of unlabeled (a) and globally ^{15}N-labeled (b) PSII complexes and of PSII complexes in D_2O (c), in comparison with a $Y_D^{\bullet}/Y_D$ difference spectrum (d). Ticks without labels indicate the same frequencies as in spectrum a. The spectra were measured in buffers at pH or pD 6.5. The intensity of the $Y_D^{\bullet}/Y_D$ difference spectrum (d) was multiplied by 0.25 because of its intensity greater than that of the $Y_Z^{\bullet}/Y_Z$ spectrum due to the rather stable formation of $Y_D^{\bullet}$.

conformational changes of the polypeptide main chains surrounding Y_Z. The amide II bands (NH bends and CN stretches) coupled to the amide I bands were observed at 1560, 1553, and 1544 cm^{-1}, which were confirmed by the downshifts to 1545, 1538, and 1530 cm^{-1}, respectively, by global ^{15}N substitution (Figure 3b). The ^{15}N substitution also downshifted a negative band from 1101 to 1095 cm^{-1} (Figure 3b), indicative of the presence of the His CN vibration[54,58,59] around this position (the expanded view of this region is presented in Figure 4a). Indeed, the ^{14}N-minus-^{15}N double-difference spectrum (Figure 4c, blue line) exhibited a differential signal with peaks at 1102 and 1091 cm^{-1}. It was previously shown that the extent of the deuteration shift of the His CN stretch is dependent on the protonation structure.[54] The His CN region of the $Y_Z^{\bullet}/Y_Z$ spectra measured in D_2O showed a negative band at 1108 cm^{-1} in the unlabeled sample and at 1097 cm^{-1} in the ^{15}N-substituted sample (Figure 4b), providing a differential signal at 1105/1096 cm^{-1} in the ^{14}N-minus-^{15}N double-difference spectrum (Figure 4c, green line). Thus, the His CN signal was only slightly upshifted (by 3−5 cm^{-1}) upon deuteration.

The higher-frequency region above 2200 cm^{-1} of the $Y_Z^{\bullet}/Y_Z$ spectrum (Figures 2 and 5) has not been reported previously. A broad positive feature around 2800 cm^{-1}, which begins from ~2300 cm^{-1} and continues at least to 3000 cm^{-1} (the region above 3000 cm^{-1} could not be observed because of saturation by bulk water absorption), appeared in the spectrum. On this broad feature, small peaks were observed at 2902, 2882, 2856, 2659, and 2630 cm^{-1}, which downshifted to 2871, 2857, 2836, 2640, and 2606 cm^{-1}, respectively, by 31−19 cm^{-1} upon global

dx.doi.org/10.1021/bi500237y | *Biochemistry* 2014, 53, 3131−3144

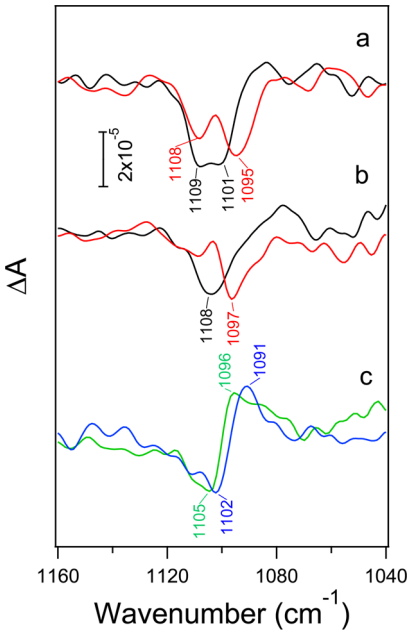

Figure 4. His CN stretching region of the $Y_Z^{\bullet}/Y_Z$ FTIR difference spectra of unlabeled (black lines) and ^{15}N-labeled (red lines) PSII complexes in H_2O (a) and D_2O (b). (c) Unlabeled-minus-^{15}N-labeled double-difference spectra in H_2O (blue) and D_2O (green). The spectra were measured in buffers at pH or pD 6.5.

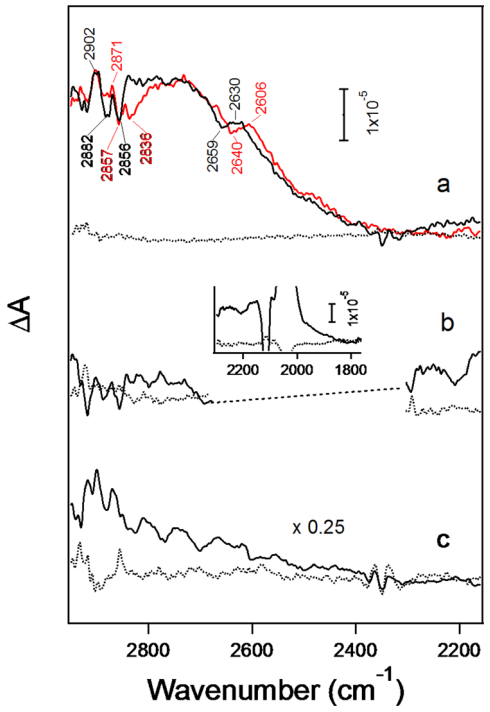

Figure 5. 2900−2200 cm^{-1} region of the $Y_Z^{\bullet}/Y_Z$ FTIR difference spectra of unlabeled (a, black line) and globally ^{15}N-labeled (a, red line) PSII complexes and of PSII complexes in D_2O (b), in comparison with a $Y_D^{\bullet}/Y_D$ difference spectrum (c). The inset shows the 2300−1800 cm^{-1} region of the $Y_Z^{\bullet}/Y_Z$ spectrum in D_2O. Dotted curves are dark-minus-dark spectra representing baselines. The region connected by a dashed line in spectrum c is saturated by the strong OD stretching bands of bulk D_2O. PSII samples are in buffers at pH or pD 6.5.

^{15}N substitution (Figure 5a). These ^{15}N-sensitive peaks in the 3000−2500 cm^{-1} region on the broad feature are similar to those previously observed in the Q_A^-/Q_A, Q_B^-/Q_B, and S_2/S_1 difference spectra,[59−63] in which the peaks have been attributed to the Fermi resonance of the overtones and combinations of the vibrations of a His side chain with its NH stretching mode. The broad feature itself also downshifted by ∼10 cm^{-1} upon ^{15}N substitution (Figure 5a). Thus, it is highly likely that the broad feature with the Fermi resonance peaks originates from the NH stretching vibration of His. This NH assignment was supported by the observation that the broad band around 2800 cm^{-1} disappeared in D_2O (Figure 5c), and instead, another broad band appeared around 2100 cm^{-1} overlapping the ferricyanide (2116 cm^{-1}) and ferrocyanide (2038 cm^{-1}) peaks (Figure 5b, inset).

The notable observation is that a similar broad feature was absent in the $Y_D^{\bullet}/Y_D$ spectrum (Figure 5c). The gradually increasing intensity from ∼2600 cm^{-1} to the higher frequency might suggest the presence of a broad band at a frequency higher than 3000 cm^{-1} overlapping the bulk water region. This gradual slope diminished in D_2O (Figure S1A of the Supporting Information, blue line), while global ^{15}N labeling did not influence the small peaks in the 2850−2600 cm^{-1} region (at 2809, 2768, 2747, and 2702 cm^{-1}) except for the minor peaks around 2600 cm^{-1} (Figure S1A of the Supporting Information, red line). Thus, this increase in the intensity of the background seems to arise mainly from a hydrogen bond network around Y_D rather than the NH of His coupled to Y_D. The small peaks may originate from the overtones and/or combinations of the fundamental vibrations of proteins but likely not from the Fermi resonance of the His vibrations.

Figure 6 presents the $Y_Z^{\bullet}/Y_Z$ spectra (A, 1800−1000 cm^{-1}; B, 3000−2200 cm^{-1}) measured at pH 7.5 (a) and pH 5.5 (c) in comparison with the spectrum at pH 6.5 (b, identical to Figures 3a and 5a, black line). A drastic change was observed at pH 5.5. The broad band around 2800 cm^{-1} disappeared at this pH, leaving small peaks at slightly different frequencies (Figure 6B, spectrum c), whereas the feature in this region was basically unchanged at pH 7.5 except for a slight increase in its intensity. The positive ν_{CO} peak of $Y_Z^{\bullet}$ at 1514 cm^{-1} was virtually identical throughout the pH range of 5.5−7.5. However, the negative ν_{CO}/δ_{COH} peak at 1256 cm^{-1} at pH 6.5 was shifted to 1259 cm^{-1} at pH 5.5, while it seems to be slightly broadened (or could be split into two peaks) at pH 7.5 (Figure 6A). These changes indicate that the hydrogen-bonded structures of Y_Z and the coupled D1-His190 are significantly different between pH 5.5 and 7.5, while the structure at pH 6.5 is mostly identical to that at pH 7.5 except for a minor mixing of the structure at pH 5.5.

Although the ν_{CO} frequency most straightforwardly reflects the hydrogen bond interaction of a Tyr side chain,[57] the coupling and overlap of the δ_{COH} vibration hamper the identification of the original ν_{CO} frequency of reduced Y_Z in the $Y_Z^{\bullet}/Y_Z$ FTIR spectra. To identify the pure ν_{CO} band of Y_Z at different pH values, $Y_Z^{\bullet}/Y_Z$ spectra were measured in D_2O buffers to remove the δ_{COH} vibration from the ν_{CO} region (Figure 7). The ν_{CO} band of reduced Y_Z was observed at 1263, 1262, and 1259 cm^{-1} at pD 7.5, 6.5, and 5.5, respectively (Figure 7C). Thus, the frequency downshifted by 4 cm^{-1} with a change in pD from 7.5 to 5.5, while only the 1 cm^{-1} shift was observed at pH 6.5. In contrast, the ν_{CO} band of $Y_Z^{\bullet}$ at 1513 cm^{-1} did not change at all (Figure 7B), in agreement with the result in H_2O (Figure 6A). These observations are consistent

dx.doi.org/10.1021/bi500237y | Biochemistry 2014, 53, 3131−3144

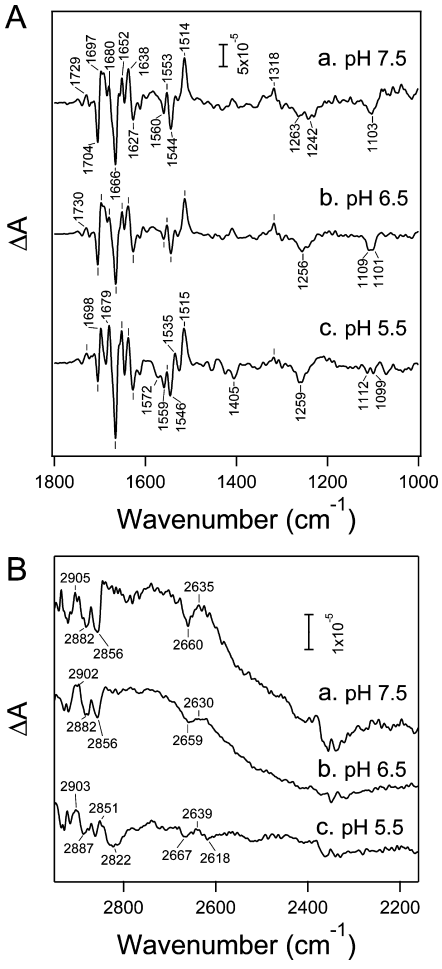

Figure 6. pH dependence of the $Y_Z^{\bullet}/Y_Z$ FTIR difference spectra in the regions of 1800−1000 cm^{-1} (A) and 2900−2200 cm^{-1} (B) at pH 7.5 (a), pH 6.5 (b), and pH 5.5 (c). The spectra at pH 6.5 (b) are identical to the spectra in Figures 3a and 5a (black line). The structures around 2350 cm^{-1} (in spectra a and c in panel B) are artifacts of CO_2 absorption. Ticks without labels indicate the same frequencies as in spectrum a.

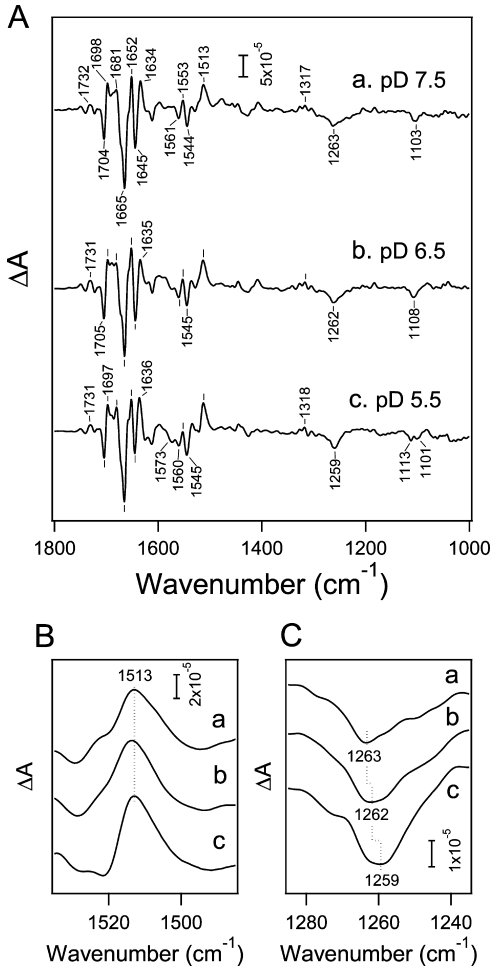

Figure 7. pD dependence of the $Y_Z^{\bullet}/Y_Z$ FTIR difference spectra in D_2O buffers in the 1800−1000 cm^{-1} region (A) and the expanded views of the ν_{CO} bands of $Y_Z^{\bullet}$ (B) and Y_Z (C) at pD 7.5 (a), pD 6.5 (b), and pD 5.5 (c). The spectrum at pD 6.5 (b) is identical to the spectrum in Figure 3c. Ticks without labels indicate the same frequencies as in spectrum a.

with the view that the hydrogen-bonded structure of reduced Y_Z is changed so that the C−O bond is weakened as the pH or pD is decreased from 7.5 to 5.5, whereas that of oxidized $Y_Z^{\bullet}$ is unchanged.

To further investigate the origin of the broad feature in the $Y_Z^{\bullet}/Y_Z$ spectrum and the hydrogen-bonded structures of Y_Z and Y_D and their coupled His, DFT and QM/MM calculations of the Y_Z-His and Y_D-His pairs were performed. In DFT calculations, *p*-cresol and 4-MeIm were used as models of Tyr and His side chains (Figure 8), respectively. The imidazole group of the His side chain has four protonation structures, i.e., the two neutral tautomers (N_τ-H and N_π-H forms) and the protonated imidazolium cation and deprotonated imidazolate anion forms. Because there are many combinations of the protonation and hydrogen-bonded structures in Tyr-His complexes, we assumed the most probable models for Y_Z, $Y_Z^{\bullet}$, Y_D, and $Y_D^{\bullet}$, taking into consideration the interactions with surrounding amino acids, and examined the agreement of the calculated results with the experimental data. N_π of D1-His190 coupled to Y_Z is within hydrogen bonding distance (2.60 Å) of the amide oxygen of D1-Asn298 in the X-ray structure (Figure 1A),[16] and hence, this N_π is probably protonated to form a hydrogen bond to D1-Asn298. Thus, in the oxidized $Y_Z^{\bullet}$ state, D1-His190 most likely has a $HisH^+$ cation form to have a hydrogen bond at N_τ-H with the deprotonated oxygen of $Y_Z^{\bullet}$ (Figure 8a). In the reduced Y_Z state, there are two possibilities. (1) His has a neutral N_π-H form, and the OH of Y_Z is hydrogen bonded to N_τ of His (Figure 8b). (2) His has a $HisH^+$ cation form, and its N_τ-H is hydrogen bonded to the oxygen atom of Y_Z OH (Figure 8c). The latter structure may be realized at lower pH values. In contrast to Y_Z, N_π of D2-His189 coupled to Y_D is within hydrogen bonding distance (2.81 Å) of N_ε of the guanidinium cation of D2-Arg294 (Figure 1B), and hence, N_π of this His is probably deprotonated to accept a hydrogen bond from this Arg.[31] Thus, D2-His189 probably has a neutral N_τ-H form in both the $Y_D^{\bullet}$ and Y_D states to donate a hydrogen bond to the deprotonated and protonated oxygen, respectively, of Tyr (Figure 8d,e).

In the QM/MM calculations of the Y_Z-His site, D1-Asn298, D1-Gln165, Ca, and 11 nearby water molecules along with Y_Z and D1-His190 were assigned to the QM region (Figure S2 of the Supporting Information) and the surrounding moieties (including the Mn and Cl^- ions) were treated as a MM region. Note that geometry optimization of the QM region in the reduced Y_Z state did not significantly change the positions of

dx.doi.org/10.1021/bi500237y | *Biochemistry* 2014, 53, 3131−3144

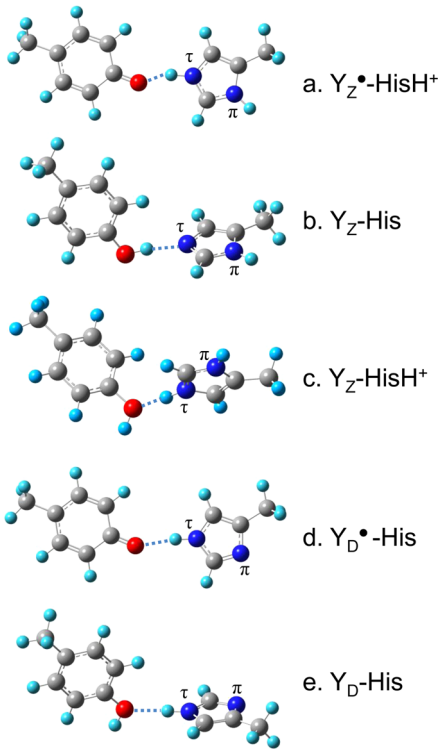

Figure 8. Optimized geometries of the model complexes of Y_Z and Y_D coupled with His obtained by DFT calculations: (a) $Y_Z^{\bullet}$-HisH$^+$, (b) Y_Z-His, (c) Y_Z-HisH$^+$, (d) $Y_D^{\bullet}$-His, and (e) Y_D-His. *p*-Cresol and 4-methylimidazole were used as models of $Y_{Z(D)}$ and a histidine side chain, respectively.

the heavy atoms, especially those of water oxygens, from the initial positions taken from the 1.9 Å X-ray structure[16] (Figure S2c of the Supporting Information). For the Y_D-His site, Y_D, D2-His189, D2-Arg294, D2-Arg180, and a water molecule interacting Y_D were assigned to the QM region (Figure S3 of the Supporting Information).

The calculated frequencies of the N_τ-H stretching vibration of His together with the O···N_τ hydrogen bond distances are summarized in Table 1 (the coordinates of optimized geometries are listed in Table S1 of the Supporting Information). The QM/MM calculation of Y_Z (Figure S2b of the Supporting Information) provided a short O···N_τ distance of 2.49 Å, which is consistent with the distance in the X-ray structure (2.46 Å)[16] as well as in the previous QM/MM calculation (2.47 Å),[17] although the DFT calculation showed a longer distance of 2.82 Å. The relatively long O···N_τ distance in Y_D-His as determined by DFT (3.02 Å) and QM/MM (2.79 Å) calculations is also consistent with that in the X-ray structure (2.74 Å).[16] Thus, the hydrogen bonding interactions between $Y_{Z\ (D)}$ and the coupled His were satisfactorily reproduced in calculations.

The frequency of the N_τ-H vibration, which is a significantly localized mode (Figure S4 of the Supporting Information), of the $Y_Z^{\bullet}$-HisH$^+$ model was calculated at 2810 cm^{-1} in the DFT calculation (Table 1). In the QM/MM calculation of $Y_Z^{\bullet}$-HisH$^+$, the symmetric and asymmetric N_τ-H/N_π-H stretching vibrations were calculated at 2986 and 2748 cm^{-1}, respectively, the latter having a high intensity. These values are significantly lower than the N_τ-H frequencies of free 4-MeIm and 4-MeImH$^+$ (3601−3546 cm^{-1}), and the IR intensities are much larger than those in the latter free molecules (Table 1). The His side chain in Y_Z-His (Figure 8b) is deprotonated at N_π, and hence, there is no N_τ-H vibration; Y_Z-HisH$^+$ (Figure 8c) showed a relatively low N_τ-H frequency of 3027 cm^{-1}. In all of the Y_Z models, ^{15}N substitution downshifts the N-H frequencies by 9−11 cm^{-1} (not shown in the table). In contrast to $Y_Z^{\bullet}$ and Y_Z, $Y_D^{\bullet}$-His and Y_D-His (Figure 8d,e) exhibited relatively high N_τ-H frequencies (3417−3162 and 3534−3250 cm^{-1}, respectively) in the DFT and QM/MM calculations.

Table 1. N_τ-H Stretching Frequencies (cm^{-1}) of the His Coupled to Y_Z and Y_D Estimated by DFT and QM/MM Calculations

	calculation			experimental	
	method	frequency (IR intensity)[a]	$r_{O\cdots N_\tau}$ (Å)[b]	frequency[c]	$r_{O\cdots N_\tau}$ (Å)[b]
$Y_Z^{\bullet}$-HisH$^+$	DFT	2810 (4569)	2.63	∼2800	
	QM/MM	2986 (1390)/ 2748 (3554)[d]	2.63		
$Y_Z^{\bullet}$-HisD$^+$[e]	DFT	2106 (2154)	–	∼2100	
Y_Z-His	DFT	–	2.82		2.46[f]
	QM/MM	–	2.49		
Y_Z-HisH$^+$	DFT	3027 (2211)	2.75		
$Y_D^{\bullet}$-His	DFT	3417 (1141)	2.95		
	QM/MM	3162 (2083)	2.77		
Y_D-His	DFT	3511 (648)	3.02		2.74[f]
	QM/MM	3250 (1490)	2.79		
4-MeIm (N_τ-H)	DFT	3601 (58)			
4-MeImH$^+$	DFT	3554 (72)/3546 (281)[d]			

[a]IR intensity calculated in kilometers per mole. [b]Hydrogen bond distance between the oxygen atom of Tyr and N_τ of His. [c]Experimental frequency observed in this study. [d]Coupled symmetric and asymmetric stretching vibrations of N_τ-H and N_π-H. [e]The exchangeable protons of N_τ-H and N_π-H of HisH$^+$ are deuterated. [f]Value from the X-ray structure of PSII (PDB entry 3ARC[16]).

These calculated N_τ-H frequencies are consistent with the experimental data (Table 1). The presence of a broad positive band around ∼2800 cm^{-1} in the $Y_Z^{\bullet}/Y_Z$ spectrum (Figures 2, 5, and 6) is in agreement with the strong N_τ-H (or coupled N_τ-H/N_π-H) vibration calculated at 3000−2700 cm^{-1} in $Y_Z^{\bullet}$-HisH$^+$ and the absence of the N_τ-H vibration in Y_Z-His. The downshift of the broad band to ∼2100 cm^{-1} in the D_2O measurements (Figure 5b, inset) was also reproduced by the frequency of deuterated $Y_Z^{\bullet}$-HisD$^+$ at 2106 cm^{-1} in the DFT calculation (Table 1), while the ^{15}N-induced downshift of ∼10 cm^{-1} (Figure 5a) is in agreement with the calculated shift. In addition, the absence of a broad band at pH 5.5 (Figure 6Bc) is consistent with the calculated low frequency of N_τ-H at ∼3000 cm^{-1} in Y_Z-HisH$^+$, which may cancel the positive band of $Y_Z^{\bullet}$-HisH$^+$. Furthermore, the calculated frequency of $Y_D^{\bullet}$-His at 3417−3162 cm^{-1} is in agreement with the observation that the $Y_D^{\bullet}/Y_D$ spectrum did not show a positive band in the region lower than 3000 cm^{-1} except for a baseline rise (Figure 5c).

Table 2 presents the calculated frequencies of the CN stretching vibration of His in the Y_Z-His pair. The frequencies were estimated to be ∼1100 cm^{-1}, in agreement with the experimental results (Figure 4). The HisH$^+$ form in $Y_Z^{\bullet}$-HisH$^+$ shows a CN frequency lower than that of the neutral N_π-H form in Y_Z-His, consistent with the previous calculated and experimental data of free His or 4-MeIm.[54,58,59] The CN frequencies are downshifted by ^{15}N substitution by 4−7 and 2−

dx.doi.org/10.1021/bi500237y | *Biochemistry* 2014, 53, 3131−3144

Table 2. CN Stretching Frequencies (cm^{-1}) of His Coupled to Y_Z Estimated by DFT and QM/MM Calculations

		protonated		deuterated[a]		
		frequency (^{15}N shift)[b]	IR intensity[c]	frequency (^{15}N shift)[b]	IR intensity[c]	H/D shift[d]
DFT	Y_Z-His	1121 (−7)	54	1120 (−6)	48	−1
	$Y_Z^{\bullet}$-$HisH^+$	1097 (−5)	3	1113 (−4)	7	+16
QM/MM	Y_Z-His	1109 (−4)	94	1112 (−4)	114	+3
	$Y_Z^{\bullet}$-$HisH^+$	1086 (−3)	18	1103 (−2)	7	+17

[a]All the exchangeable protons are deuterated. [b]All the nitrogen atoms in His (DFT) and in the QM region (QM/MM) are substituted with ^{15}N. [c]IR intensity calculated in kilometers per mole. [d]Frequency shift upon deuteration.

5 cm^{-1} in Y_Z-His and $Y_Z^{\bullet}$-$HisH^+$, respectively. Upon deuteration, Y_Z-His shows only a minor shift between −1 and 3 cm^{-1}, whereas $Y_Z^{\bullet}$-$HisH^+$ shows a large upshift of 16−17 cm^{-1}, which is in agreement with the previous calculation for free 4-MeIm.[54] It is notable, however, that the IR intensities of the protonated $HisH^+$ form in $Y_Z^{\bullet}$-$HisH^+$ are much smaller than those of neutral His in Y_Z-His by factors of 5−18 in DFT and QM/MM calculations, suggesting that the His bands of the reduced Y_Z-His state mainly appear in the $Y_Z^{\bullet}/Y_Z$ spectrum. These calculated results are quite consistent with the experimental spectra in Figure 4. The major contribution is a negative band due to the reduced Y_Z-His, which showed a ^{15}N downshift by ~6 cm^{-1} (Figure 4a), indicative of the change of the neutral N_π-H form of His to another form upon formation of $Y_Z^{\bullet}$. The upshift of 3−5 cm^{-1} upon deuteration (Figure 4c) is also consistent with the minor deuteration effect of the reduced Y_Z-His (Table 2). The CN band of the $HisH^+$ form in $Y_Z^{\bullet}$-$HisH^+$, which should show a large deuteration shift of 16−17 cm^{-1}, was not identified in the observed FTIR spectra, which is also consistent with the significantly smaller intensity and a slightly smaller ^{15}N shift estimated by calculations. Thus, the FTIR spectra in the His CN region together with DFT and QM/MM calculations support the view that the protonation structure of the His coupled to Y_Z is changed from the neutral N_π-H form to the protonated cation form upon Y_Z oxidation.

The QM/MM calculations for the Y_Z site also exhibited a significant rearrangement of the hydrogen bond network around Y_Z concomitant with the movements of water molecules upon Y_Z oxidation (Figure 9). When Y_Z is oxidized, a proton of Y_Z is released to N_τ of D1-His190, forming a strong hydrogen bond with a neutral $Y_Z^{\bullet}$ radical. Because the CO bond of the $Y_Z^{\bullet}$ radical has a double bond character [the CO stretching vibration is significantly upshifted from 1262 to 1513 cm^{-1} (Figure 7)], the Y_Z oxygen can accept only two hydrogen bonds. Hence, the hydrogen bond with the W4 proton, which is weaker than that with W7,[17] is broken, and this proton turns to the side of another water molecule (designated W_A in Figure 9). This rotation of W4 induces the movement of W_A toward D1-His190. The distance between the W_A oxygen and N_τ of D1-His190 is shortened from 4.57 to 3.28 Å upon Y_Z oxidation. A network of water molecules is now formed from W4 to W_D through W_A, W_B, and W_C near D1-Asn298 (Figure 9) and is further connected to the hydrogen bond network to the lumenal side.[16]

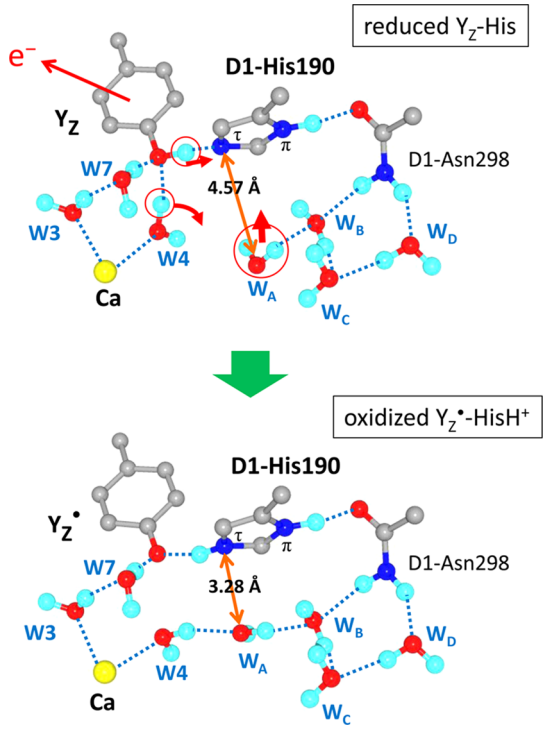

Figure 9. Rearrangement of the hydrogen bond network near Y_Z upon its oxidation estimated by QM/MM calculations. Relevant amino acid side chains, water molecules, and the Ca atom were selected from the QM region (Figure S2 of the Supporting Information). In the amino acid side chains, hydrogen atoms other than exchangeable protons have been omitted. The drastic movements of protons and a water molecule are expressed with red circles and red arrows. Upon Y_Z oxidation, the Y_Z proton is shifted to D1-His190, the hydrogen bond of the W4 proton with the Y_Z oxygen is broken and this proton is turned to the W_A side to form a new hydrogen bond, and W_A moves toward D1-His190.

DISCUSSION

Upon oxidation of Y_Z, a proton is released from the phenolic OH to from a neutral radical $Y_Z^{\bullet}$.[11−13,18,64] This FTIR study directly detected this proton that is trapped by the neighboring His residue, D1-His190, as an N_τ-H stretching vibration. The broad positive feature around 2800 cm^{-1} in the $Y_Z^{\bullet}/Y_Z$ FTIR difference spectrum (Figures 2, 5, and 6) was assigned to this N_τ-H vibration (or the coupled N_τ-H/N_π-H vibration) of the protonated $HisH^+$ cation. The evidence of this assignment was obtained from isotopic substitutions and quantum chemical calculations. H/D exchange induced a large downshift from ~2800 to ~2100 cm^{-1} (Figure 5b), indicative of the vibration involving an exchangeable proton. In addition, global ^{15}N substitution showed downshifts of the broad feature and superimposing several small peaks on it (Figure 5a), indicating the presence of the NH vibration coupled with other His vibrations by Fermi resonance. The DFT calculation of the $Y_Z^{\bullet}$-$HisH^+$ model (Figure 8a) and the QM/MM calculation taking into account the surrounding amino acids and water molecules (Figure S2a of the Supporting Information) provided the N_τ-H stretching vibration or the coupled N_τ-H/N_π-H vibrations of $HisH^+$ at 3000−2700 cm^{-1} (Table 1), reproducing the

dx.doi.org/10.1021/bi500237y | Biochemistry 2014, 53, 3131−3144

observed frequency well. The absence of protonated N_τ-H in the reduced Y_Z-His form (Figure 8b) rationalizes the appearance of a positive N_τ-H band of $HisH^+$ in the $Y_Z^\bullet/Y_Z$ difference spectrum. In addition, the DFT calculation of deuterated $Y_Z^\bullet$-$HisD^+$ providing the N_τ-D frequency of 2106 cm^{-1} (Table 1) reproduced a downshift to ~2100 cm^{-1} in D_2O (Figure 4c, inset). Furthermore, the results of the analysis of the CN stretching vibration of His using ^{15}N substitution and deuteration (Figure 4) in combination with DFT and QM/MM calculations (Table 2) are consistent with the change in the protonation structure of His from the neutral N_π-H form to the protonated cation form upon $Y_Z^\bullet$ formation.

The pH dependence of the $Y_Z^\bullet/Y_Z$ spectrum further supported the assignment given above. The positive feature around ~2800 cm^{-1} disappeared at pH 5.5 (Figure 6Bc). The DFT calculation of the reduced Y_Z-$HisH^+$ (Figure 8c), which is thought to be formed at lower pH values (Figure 10),[12,18,24,64]

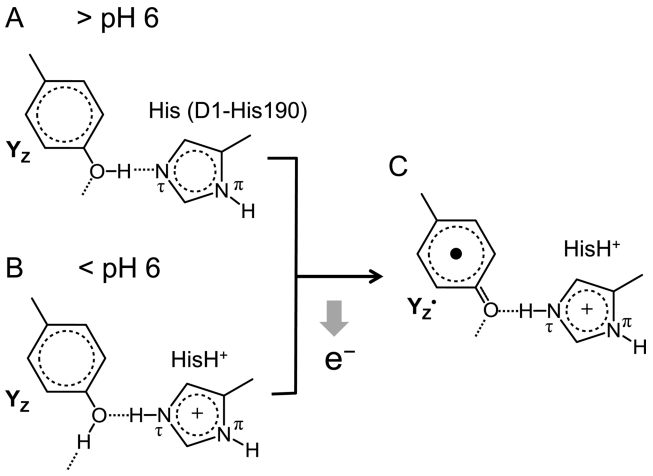

Figure 10. Changes in the hydrogen-bonded structures of Y_Z and D1-His190 with pH and photooxidation.

showed a relatively low N_τ-H frequency of 3027 cm^{-1} (Table 1), comparable to the calculated frequencies at 3000−2700 cm^{-1} of $Y_Z^\bullet$-$HisH^+$. Thus, the absence of the band is explained by cancellation of the N_τ-H band in the difference spectrum between Y_Z-$HisH^+$ and $Y_Z^\bullet$-$HisH^+$. The change in the hydrogen-bonded structure of reduced Y_Z at a low pH (Figure 10A,B) was confirmed by the downshift of the pure ν_{CO} band of Y_Z, which was decoupled from the δ_{COH} vibration by measurement in D_2O, from 1263 cm^{-1} at pD 7.5 to 1259 cm^{-1} at pD 5.5 (Figure 7C). In contrast, the ν_{CO} frequency of oxidized $Y_Z^\bullet$ was virtually unchanged throughout the pH or pD range of 5.5−7.5 (Figures 6A and 7B), consistent with the view that $Y_Z^\bullet$ has a structure identical to that of $Y_Z^\bullet$-$HisH^+$ over this pH or pD range (Figure 10C). If the structural models in Figure 10 are correct, a proton should be released from the Y_Z-His moiety at pH 5.5. Indeed, at this pH, negative bands at 1405 and 1572 cm^{-1}, which can be interpreted as arising from the symmetric and asymmetric carboxylate stretching vibrations, respectively, and a positive feature around 1720 cm^{-1} that can be attributed to the C=O stretches of protonated COOH groups were observed (Figure 6A, spectrum c), suggesting that some specific or nonspecific caroboxylate groups in PSII proteins were protonated by the proton released from Y_Z. Our observation indicates that the pK_a of D1-His190 coupled to the reduced Y_Z is around 6 in our core complexes from *T. elongatus*. Although this value is lower than the general pK_a estimation (~7) in Mn-depleted PSII preparations in previous reports,[12,18,64] it has also been shown that the pK_a of this His is significantly dependent on the PSII preparations and the content of metal ions.[24,64]

In contrast to $Y_Z^\bullet$, $Y_D^\bullet$ did not show a broad band at ~2800 cm^{-1} at pH 6.5 (Figure 5c) or even at pH 10.5 (data not shown). Indeed, the DFT and QM/MM calculations of the $Y_D^\bullet$-His (Figure 8d and Figure S3a of the Supporting Information) and Y_D-His (Figure 8e and Figure S3b of the Supporting Information) models, in which His has a neutral N_τ-H form, provided the N_τ-H frequencies at much higher frequencies of 3550−3150 cm^{-1} (Table 1), the region of strong water bands. Thus, these calculations also explain well the $Y_D^\bullet/Y_D$ FTIR spectrum, supporting the assignment of the N-H band at ~2800 cm^{-1} in the $Y_Z^\bullet/Y_Z$ spectrum described above.

All of the FTIR data provided above and the results of DFT and QM/MM calculations indicate that D1-His190 coupled with the oxidized $Y_Z^\bullet$ radical has a protonated cation form. The low N-H frequency of ~2800 cm^{-1} reflects the presence of a strong hydrogen bond between $Y_Z^\bullet$ and $HisH^+$. Because the similar hydrogen bond with a neutral His in the $Y_D^\bullet$-His model showed a higher N_τ-H frequency (3417−3162 cm^{-1}) and a longer O···N_τ distance (2.77−2.96 Å in comparison with 2.63 Å in $Y_Z^\bullet$-$HisH^+$) (Table 1), this strong hydrogen bonding interaction of $Y_Z^\bullet$-$HisH^+$ most probably originates from the so-called charge-assisted hydrogen bond.[65−67] The stronger hydrogen bond in $Y_Z^\bullet$ compared with that in $Y_D^\bullet$ has also been pointed out in the ν_{CO} frequency in $Y_Z^\bullet$ (1514 cm^{-1}) being higher than that in $Y_D^\bullet$ (1504 cm^{-1}) (Figure 3).[44] Theoretical calculations have shown that a stronger hydrogen bond upshifts the ν_{CO} frequency of the $Tyr^\bullet$ radical.[68,69] The retention of a positive charge on D1-His190 after Y_Z oxidation is consistent with the previous reports of the electrochromic shift of Chl absorption upon Y_Z oxidation,[20] the low g_x value in the high-field EPR spectrum,[22] the absence of proton release,[24] and the Y_Z oxidation capability at ultralow temperatures.[12]

The N-H band around ~2800 cm^{-1} in the $Y_Z^\bullet/Y_Z$ spectrum has a very broad width (Figures 2 and 5a). This type of broad feature in IR spectra has been attributed to a strong hydrogen bond with large proton polarizability, and the crucial role of such a polarizable proton in proton transfer in proteins has been proposed.[70−74] The broad N-H band of $Y_Z^\bullet$ indicates that the proton in the strong hydrogen bond between $Y_Z^\bullet$ and $HisH^+$ is highly polarizable; i.e., it readily moves in response to the change in the electrostatic field in the environment. The presence of a polarizable proton in the hydrogen bond of $Y_Z^\bullet$ is also consistent with the slightly broader ν_{CO} band at 1514 cm^{-1} in comparison with that at 1504 cm^{-1} in $Y_D^\bullet$ (Figure 3), the observation previously mentioned by Berthomieu et al.[44]

We used the Mn-depleted PSII core complexes for the measurement of $Y_Z^\bullet/Y_Z$ FTIR difference spectra in this study. The property of Y_Z is predicted to be changed by Mn depletion.[13,64] In particular, the structure of the water cluster near the Ca atom and Y_Z (Figure 1) may be broken upon removal of the Mn_4Ca cluster. However, the QM/MM calculation including water molecules and amino acid residues surrounding Y_Z as the QM region provided an N-H frequency (2748 cm^{-1}) similar to that determined by the DFT calculation (2810 cm^{-1}) without these groups (Table 1). Experimentally, the high-field EPR study using a PSII crystal also showed that the orientation of Y_Z does not change after Mn depletion and thus concluded that the pattern of hydrogen bonding around

dx.doi.org/10.1021/bi500237y | *Biochemistry* 2014, 53, 3131−3144

$Y_Z^\bullet$ is not influenced drastically by removal of the Mn_4Ca cluster.[22] Also, it was shown that at alkaline pH values, Mn-depleted PSII is significantly kinetically similar to intact PSII, indicative of the same reaction mechanism of PCET of Y_Z.[18] Furthermore, the recent time-resolved IR measurements of intact PSII complexes exhibited a positive signal at 2500 cm^{-1} in the time region of several microseconds,[75] at which $Y_Z^\bullet$ mainly accumulates, indicating the presence of a positive intensity at 2500 cm^{-1} in the $Y_Z^\bullet$ IR spectrum of the intact PSII. Therefore, the conclusion about the hydrogen bonding interaction between $Y_Z^\bullet$ and D1-His190 obtained using Mn-depleted PSII should basically hold also in Mn-intact PSII.

It is noted that a broad positive feature with several peaks in the 3000−2500 cm^{-1} region has also been observed in the S_2/S_1 difference spectrum of the water-oxidizing center.[59,76] We previously showed that these peaks on the broad feature in the 2850−2500 cm^{-1} region originate from the Fermi resonance of the His side chain(s) using global ^{15}N and [^{15}N]His substitutions,[59] while the underlying broad feature was attributed to the polarizable proton in a hydrogen bond network around the Mn_4Ca cluster.[59,76] Recently, Polander and Barry[77] reported that the band at 2880 cm^{-1} in the S_2/S_1 spectrum arises from a cationic water cluster. As shown in Figure S5 of the Supporting Information, in which our previous data[59,76,78] are reorganized, the corresponding band at ∼2900 cm^{-1} clearly downshifts upon global ^{15}N and ^{13}C labeling but is unchanged by $H_2{}^{18}O$ substitution, indicating that the band at ∼2900 cm^{-1} in the S_2/S_1 difference spectrum probably arises from the Fermi resonance of the His vibrations like other peaks in the 3000−2500 cm^{-1} region. The authors mentioned above also showed the spectra of ammonia-treated and Sr^{2+}-substituted PSII samples, which diminished the intensity of the 2880 cm^{-1} band, as evidence of the assignment of the band to the cationic water cluster.[77] Our corresponding spectra (Figure S5b,f of the Supporting Information), however, show that the band feature in this region is basically unchanged by these treatments.[79,80] Thus, there is no experimental basis for the assignment of the band at ∼2900 cm^{-1} to the cationic water cluster. It is likely, however, that the broad feature in the S_2/S_1 spectrum originates from polarizable protons in the water cluster (but not cation) near Ca and Y_Z (Figure 1A), and it is presumed that the formation of a positive charge on the Mn_4Ca cluster in the $S_1 \rightarrow S_2$ transition induces the intensified IR bands of the vibrations of these polarizable protons.

The similar assignment of the broad feature at ∼2800 cm^{-1} in the $Y_Z^\bullet/Y_Z$ spectrum to the polarizable protons in the water cluster near Y_Z is unlikely because the present $Y_Z^\bullet/Y_Z$ spectrum was measured with the Mn-depleted PSII preparations. As mentioned above, depletion of the Mn_4Ca cluster will break the solid network of the water cluster near Ca and Y_Z, and hence, Y_Z may be surrounded by loosely bound water molecules similar to bulk water, which shows the OH bands at ∼3400 cm^{-1}. The observed ^{15}N shift (Figure 5a) and the disappearance of the broad feature at pH 5.5 (Figure 6Bc) also cannot be explained by the water cluster as the origin of the broad feature. It is possible, however, that the bands of polarizable protons in the water cluster superimpose the N-H band of $HisH^+$ when a $Y_Z^\bullet/Y_Z$ spectrum is obtained in Mn_4Ca-intact PSII preparations. Future time-resolved IR studies using intact PSII will clarify this point.

The role of a positive charge on D1-His190 next to the $Y_Z^\bullet$ radical in the water oxidation mechanism has been proposed to be driving the release of the proton from substrate water especially in the S_2 and S_3 states, which has the surplus of a positive charge on the Mn_4Ca cluster.[12,32,34,81] On the other hand, retention of the proton at N_τ of D1-His190 without proton release even from N_π-H is at odds with the previous proposal of the "hydrogen abstraction model",[19] in which a proton is first released from the Y_Z site to the lumen and then the $Y_Z^\bullet$ radical abstracts a hydrogen atom from substrate water. The arguments against this model have already been made by many authors from experimental[12,20−22] and theoretical[82] viewpoints. The data in this FTIR study add further evidence that opposes this model. There is another possibility, however, that Y_Z is directly related to proton transfer without releasing a proton upon its oxidation: the Y_Z-His site is simply involved in a proton transfer pathway when a proton is released from substrate water in some S-state transitions.

From the information of the X-ray structure of PSII,[14−16] possible proton pathways have been predicted.[16,25−27,83] The most probable pathway is the one that starts from D1-Asp61 and passes through Cl-1.[35,36,83−90] The hydrogen bond network connecting Y_Z and the lumen was also proposed as a candidate of the proton pathway.[16,27] There is a water cluster between the Mn_4Ca cluster and Y_Z (Figure 1A), and thus, the protons of the water ligands, W4, W3, and W2 (and possibly O5, if this is a hydroxide[16]), are readily transferred to the Y_Z oxygen by the Grotthuss mechanism[91,92] (Figure 11). The "gate" of this proton transfer pathway is the Y_Z-His site that connects the water cluster with the water channel near D1-Asn298 leading to the lumen. The QM/MM calculations showed that upon Y_Z oxidation and concomitant release of a proton to D1-His190, the hydrogen bond between W4 and Y_Z is broken and the W4 proton forms a new hydrogen bond with another water, W_A (Figure 9). By this hydrogen bond formation, W_A significantly moves toward D1-His190 and the distance between N_τ of His190 and the W_A oxygen is shortened from 4.57 to 3.28 Å. Because the proton of N_τ-H of D1-His190 is highly polarizable (see above), it is movable responding to the change in the charge distribution in the Mn_4Ca cluster and the fluctuation of the protein and water environments, and hence, there is a

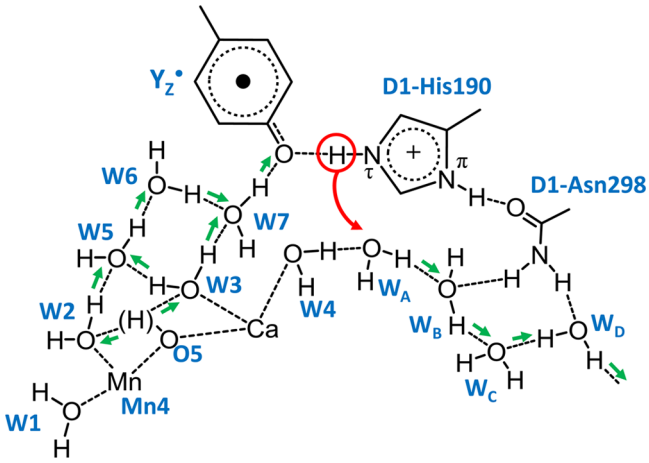

Figure 11. Proposed mechanism for the proton release from substrate water on the Mn_4Ca cluster via the $Y_Z^\bullet$-$HisH^+$ moiety as a gate. The high-polarizability proton detected in this study is marked with a red circle. Hopping of this proton to W_A, which moved toward D1-His190 upon Y_Z oxidation (Figure 9), triggers immediate transfer of a proton from substrate water to Y_Z through the water cluster by the Grotthuss mechanism (green arrows).

dx.doi.org/10.1021/bi500237y | *Biochemistry* 2014, 53, 3131−3144

chance to hop to W_A, the nearby proton acceptor. This proton hopping is the rate-limiting step and triggers the shift of the equilibrium of proton transfer between the water ligands and $Y_Z^•$ to the $Y_Z^•$ side, while the proton on W_A is also transferred to the hydrogen bond network near D1-Asn298 via water molecules (Figures 9 and 11). Thus, eventually a proton is transferred from substrate water to the lumen. An alternative possibility could be hopping of a proton from W7 to W4 (the distance between their oxygen atoms is 3.84 Å in the $Y_Z^•$ state), which is now connected to the hydrogen bond network to the lumen through W_A−W_D (Figures 9 and 11). The key event in this novel proton transfer mechanism is the movement of a water molecule for rearrangement of the hydrogen bond network. The significance of such mobile water in proton pathways has been suggested previously.[27,36,74]

This type of proton transfer can take place before the transfer of an electron from the Mn_4Ca cluster to $Y_Z^•$. Such a proton-first PCET reaction has been proposed to occur at the S_2 and S_3 states, which have an excess positive charge on the Mn_4Ca cluster, to decrease the redox potentials before electron transfer.[32,34,75,93] Which proton pathway is preferentially used in each S-state transition may depend on the structural relationship of the proton-releasing substrate with the hydrogen bond network around the Mn_4Ca cluster. The $S_3 \rightarrow S_0$ transition seems to use the pathway via D1-Asp61 and Cl-1,[35,36,83−90] because mutations at D1-Asp61[88−90] and D2-Lys317,[86,87] which is a ligand to Cl-1, retard the rate of this transition or affects the efficiency. In contrast, in the $S_2 \rightarrow S_3$ transition, another pathway near Y_Z was proposed to be active.[32] It is suggested that the electrostatic repulsion between the positive charges on D1-His190 and the Mn_4Ca cluster in the S_2 state promotes the proton transfer cascade starting from the release of the polarizable proton in $Y_Z^•$-$HisH^+$. In this case, the protons from W4, W3, and W2 (and possibly O5) can be released to the lumenal side using the proton transfer mechanism mentioned above (Figure 11). The proton transfer via $Y_Z^•$-$HisH^+$ may also take place in concerted PCET. This proton transfer mechanism looks similar to the previous hydrogen abstraction model.[19] The basic difference, however, is that in the mechanism proposed here, the triggering reaction of the transfer of a proton from $HisH^+$ determines the rate of the whole PCET process and the stable formation of deprotonated $Y_Z^•$-His is not required.

Proton rocking along the hydrogen bond between Y_Z and D1-His190 without further proton release is the most effective way to decrease the energy barrier of the redox reactions of Y_Z. The strong hydrogen bond in the Y_Z-His pair in the oxidized form as shown in this study as well as in the reduced form as theoretically revealed by Saito et al.[17] particularly contributes to the increase in the rates of Y_Z reactions. In contrast, the absence of proton rocking between Y_D and D2-His189 was also confirmed by the absence of a broad feature at a frequency of <3000 cm^{-1} (Figure 3d), indicative of no formation of the Y_D-$HisH^+$ form. This is because D2-His189 has a neutral N_τ-H form by accepting a hydrogen bond at the N_π site from the guanidinium cation of D2-Arg294 and hence cannot accept a hydrogen bond at N_τ from the Y_D OH (Figure 8e). Thus, Y_D releases a proton along a longer proton pathway in the protein, as recently indicated by the QM/MM calculations.[31] Such a difference in the proton release mechanism provides a major cause for the kinetic difference between Y_Z and Y_D[11−13] and hence their roles as the main and peripheral electron donor, respectively, to $P680^+$.

■ ASSOCIATED CONTENT

Supporting Information

$Y_D^•/Y_D$ difference spectra of ^{15}N-labeled and H/D-exchanged PSII, optimized structures of the QM regions of the Y_Z-His and Y_D-His sites in the QM/MM calculations, vector expression of the N-H stretching mode, FTIR bands around 2900 cm^{-1} in the S_2/S_1 difference spectra of PSII with various treatments, and coordinates of the optimized geometries of the Y_Z-His and Y_D-His sites obtained by DFT and QM/MM calculations. This material is available free of charge via the Internet at http://pubs.acs.org.

■ AUTHOR INFORMATION

Corresponding Author

*Phone: +81-52-789-2881. Fax: +81-52-789-2883. E-mail: tnoguchi@bio.phys.nagoya-u.ac.jp.

Funding

This study was supported by the Grants-in-Aid for Scientific Research from the Ministry of Education, Culture, Sports, Science and Technology (23657099, 24000018, 24107003, and 25291033).

Notes

The authors declare no competing financial interest.

■ ACKNOWLEDGMENTS

Computations were partly performed using the Research Center for Computational Science, Okazaki, Japan.

■ ABBREVIATIONS

Chl, chlorophyll; DFT, density functional theory; DM, *n*-dodecyl *β*-D-maltoside; FTIR, Fourier transform infrared; Hepes, 4-(2-hydroxyethyl)-1-piperazineethanesulfonic acid; IR, infrared; MeIm, methylimidazole; Mes, 2-(*N*-morpholino)-ethanesulfonic acid; ONIOM, our own *n*-layered integrated molecular orbital and molecular mechanics; PDB, Protein Data Bank; PSII, photosystem II; QM/MM, quantum mechanics/molecular mechanics.

■ REFERENCES

(1) Debus, R. J. (1992) The manganese and calcium ions of photosynthetic oxygen evolution. *Biochim. Biophys. Acta 1102*, 269−352.

(2) Hillier, W., and Messinger, J. (2005) Mechanism of photosynthetic oxygen production. In *Photosystem II: The Light-Driven Water:Plastoquinone Oxidoreductase* (Wydrzynski, T., and Satoh, K., Eds.) pp 567−608, Springer, Dordrecht, The Netherlands.

(3) McEvoy, J. P., and Brudvig, G. W. (2006) Water-splitting chemistry of photosystem II. *Chem. Rev. 106*, 4455−4483.

(4) Messinger, J., Noguchi, T., and Yano, J. (2012) Photosynthetic O_2 evolution. In *Molecular Solar Fuels* (Wydrzynski, T., and Hillier, W., Eds.) Chapter 7, pp 163−207, Royal Society of Chemistry, Cambridge, U.K.

(5) Renger, G. (2012) Photosynthetic water splitting: Apparatus and mechanism. In *Photosynthesis: Plastid Biology, Energy Conversion and Carbon Assimilation* (Eaton-Rye, J. J., Tripathy, B. C., and Sharkey, T. D., Eds.) pp 359−414, Springer, Dordrecht, The Netherlands.

(6) Grundmeier, A., and Dau, H. (2012) Structural models of the manganese complex of photosystem II and mechanistic implications. *Biochim. Biophys. Acta 1817*, 88−105.

(7) Vinyard, D. J., Ananyev, G. M., and Dismukes, G. C. (2013) Photosystem II: The reaction center of oxygenic photosynthesis. *Annu. Rev. Biochem. 82*, 577−606.

(8) Diner, B. A., and Rappaport, F. (2002) Structure, dynamics, and energetics of the primary photochemistry of photosystem II of oxygenic photosynthesis. *Annu. Rev. Plant Biol. 53*, 551−580.
(9) Renger, G., and Holzwarth, A. R. (2005) Primary electron transfer. In *Photosystem II: The Light-Driven Water:Plastoquinone Oxidoreductase* (Wydrzynski, T., and Satoh, K., Eds.) pp 139−175, Springer, Dordrecht, The Netherlands.
(10) Dixon, W. T., and Murphy, D. (1976) Determination of acidity constants of some phenol radical cations by means of electron-spin resonance. *J. Chem. Soc., Faraday Trans. 2* (72), 1221−1230.
(11) Diner, B., and Britt, R. D. (2005) The redox-active tyrosine Y_Z and Y_D. In *Photosystem II: The Light-Driven Water:Plastoquinone Oxidoreductase* (Wydrzynski, T., and Satoh, K., Eds.) pp 207−233, Springer, Dordrecht, The Netherlands.
(12) Styring, S., Sjöholm, J., and Mamedov, F. (2012) Two tyrosines that changed the world: Interfacing the oxidizing power of photochemistry to water splitting in photosystem II. *Biochim. Biophys. Acta 1817*, 76−87.
(13) Renger, G. (2012) Mechanism of light induced water splitting in Photosystem II of oxygen evolving photosynthetic organisms. *Biochim. Biophys. Acta 1817*, 1164−1176.
(14) Ferreira, K. N., Iverson, T. M., Maghlaoui, K., Barber, J., and Iwata, S. (2004) Architecture of the photosynthetic oxygen-evolving center. *Science 303*, 1831−1838.
(15) Guskov, A., Kern, J., Gabdulkhakov, A., Broser, M., Zouni, A., and Saenger, W. (2009) Cyanobacterial photosystem II at 2.9-Å resolution and the role of quinones, lipids, channels and chloride. *Nat. Struct. Mol. Biol. 16*, 334−342.
(16) Umena, Y., Kawakami, K., Shen, J. R., and Kamiya, N. (2011) Crystal structure of oxygen-evolving photosystem II at a resolution of 1.9 Å. *Nature 473*, 55−60.
(17) Saito, K., Shen, J. R., Ishida, T., and Ishikita, H. (2011) Short hydrogen bond between redox-active tyrosine Y_Z and D1-His190 in the photosystem II crystal structure. *Biochemistry 50*, 9836−9844.
(18) Rappaport, F., Boussac, A., Force, D. A., Peloquin, J., Brynda, M., Sugiura, M., Un, S., Britt, R. D., and Diner, B. A. (2009) Probing the coupling between proton and electron transfer in photosystem II core complexes containing a 3-fluorotyrosine. *J. Am. Chem. Soc. 131*, 4425−4433.
(19) Hoganson, C. W., and Babcock, G. T. (1997) A metalloradical mechanism for the generation of oxygen from water in photosynthesis. *Science 277*, 1953−1956.
(20) Rappaport, F., and Lavergne, J. (2001) Coupling of electron and proton transfer in the photosynthetic water oxidase. *Biochim. Biophys. Acta 1503*, 246−259.
(21) Junge, W., Haumann, M., Ahlbrink, R., Mulkidjanian, A., and Clausen, J. (2002) Electrostatics and proton transfer in photosynthetic water oxidation. *Philos. Trans. R. Soc., B 357*, 1407−1417.
(22) Matsuoka, H., Shen, J. R., Kawamori, A., Nishiyama, K., Ohba, Y., and Yamauchi, S. (2011) Proton-coupled electron-transfer processes in photosystem II probed by highly resolved g-anisotropy of redox-active tyrosine Y_Z. *J. Am. Chem. Soc. 133*, 4655−4660.
(23) Rappaport, F., and Lavergne, J. (1997) Charge recombination and proton transfer in manganese-depleted photosystem II. *Biochemistry 36*, 15294−15302.
(24) Ahlbrink, R., Haumann, M., Cherepanov, D., Bögershausen, O., Mulkidjanian, A., and Junge, W. (1998) Function of tyrosine Z in water oxidation by photosystem II: Electrostatical promotor instead of hydrogen abstractor. *Biochemistry 37*, 1131−1142.
(25) Ho, F. M., and Styring, S. (2008) Access channels and methanol binding site to the $CaMn_4$ cluster in Photosystem II based on solvent accessibility simulations, with implications for substrate water access. *Biochim. Biophys. Acta 1777*, 140−153.
(26) Vassiliev, S., Comte, P., Mahboob, A., and Bruce, D. (2010) Tracking the flow of water through photosystem II using molecular dynamics and streamline tracing. *Biochemistry 49*, 1873−1881.
(27) Ogata, K., Yuki, T., Hatakeyama, M., Uchida, W., and Nakamura, S. (2013) All-atom molecular dynamics simulation of photosystem II embedded in thylakoid membrane. *J. Am. Chem. Soc. 135*, 15670−15673.
(28) Boussac, A., and Etienne, A. L. (1984) Midpoint potential of signal II (slow) in Tris-washed photosystem II particles. *Biochim. Biophys. Acta 766*, 576−581.
(29) Vass, I., and Styring, S. (1991) pH-Dependent charge equilibria between tyrosine-D and the S states in photosystem II. Estimation of relative midpoint redox potentials. *Biochemistry 30*, 830−839.
(30) Metz, J. G., Nixon, P. J., Rögner, M., Brudvig, G. W., and Diner, B. A. (1989) Directed alteration of the D1 polypeptide of photosystem II: Evidence that tyrosine-161 is the redox component, Z, connecting the oxygen-evolving complex to the primary electron-donor, P680. *Biochemistry 28*, 6960−6969.
(31) Saito, K., Rutherford, A. W., and Ishikita, H. (2013) Mechanism of tyrosine D oxidation in Photosystem II. *Proc. Natl. Acad. Sci. U.S.A. 110*, 7690−7695.
(32) Klauss, A., Haumann, M., and Dau, H. (2012) Alternating electron and proton transfer steps in photosynthetic water oxidation. *Proc. Natl. Acad. Sci. U.S.A. 109*, 16035−16040.
(33) Klauss, A., Sikora, T., Süss, B., and Dau, H. (2012) Fast structural changes (200−900 ns) may prepare the photosynthetic manganese complex for oxidation by the adjacent tyrosine radical. *Biochim. Biophys. Acta 1817*, 1196−1207.
(34) Rappaport, F., Blanchard-Desce, M., and Lavergne, J. (1994) Kinetics of electron transfer and electrochromic change during the redox transitions of the photosynthetic oxygen-evolving complex. *Biochim. Biophys. Acta 1184*, 178−192.
(35) Siegbahn, P. E. M. (2012) Mechanisms for proton release during water oxidation in the S_2 to S_3 and S_3 to S_4 transitions in photosystem II. *Phys. Chem. Chem. Phys. 14*, 4849−4856.
(36) Linke, K., and Ho, F. M. (2014) Water in Photosystem II: Structural, functional and mechanistic considerations. *Biochim. Biophys. Acta 1837*, 14−32.
(37) Chu, H.-A., Hillier, W., Law, N. A., and Babcock, G. T. (2001) Vibrational spectroscopy of the oxygen-evolving complex and of manganese model compounds. *Biochim. Biophys. Acta 1503*, 69−82.
(38) Noguchi, T., and Berthomieu, C. (2005) Molecular analysis by vibrational spectroscopy. In *Photosystem II: The Light-Driven Water:-Plastoquinone Oxidoreductase* (Wydrzynski, T., and Satoh, K., Eds.) pp 367−387, Springer, Dordrecht, The Netherlands.
(39) Berthomieu, C., and Hienerwadel, R. (2005) Vibrational spectroscopy to study the properties of redox-active tyrosines in photosystem II and other proteins. *Biochim. Biophys. Acta 1707*, 51−66.
(40) Noguchi, T. (2007) Light-induced FTIR difference spectroscopy as a powerful tool toward understanding the molecular mechanism of photosynthetic oxygen evolution. *Photosynth. Res. 91*, 59−69.
(41) Debus, R. J. (2008) Protein ligation of the photosynthetic oxygen-evolving center. *Coord. Chem. Rev. 252*, 244−258.
(42) Noguchi, T. (2008) Fourier transform infrared analysis of the photosynthetic oxygen-evolving center. *Coord. Chem. Rev. 252*, 336−346.
(43) Noguchi, T. (2013) Monitoring the reactions of photosynthetic water oxidation using infrared spectroscopy. *Biomed. Spectrosc. Imaging 2*, 115−128.
(44) Berthomieu, C., Hienerwadel, R., Boussac, A., Breton, J., and Diner, B. A. (1998) Hydrogen bonding of redox-active tyrosine Z of photosystem II probed by FTIR difference spectroscopy. *Biochemistry 37*, 10547−10554.
(45) Stanier, R. Y., Kunisawa, R., Mandel, M., and Cohen-Baziere, G. (1971) Purification and properties of unicellular blue-green algae (order Chroococcales). *Bacteriol. Rev. 35*, 171−205.
(46) Iwai, M., Suzuki, T., Kamiyama, A., Sakurai, I., Dohmae, N., Inoue, Y., and Ikeuchi, M. (2010) The PsbK subunit is required for the stable assembly and stability of other small subunits in the PSII complex in the thermophilic cyanobacterium *Thermosynechococcus elongatus* BP-1. *Plant Cell Physiol. 51*, 554−560.
(47) Boussac, A., Rappaport, F., Carrier, P., Verbavatz, J. M., Gobin, R., Kirilovsky, D., Rutherford, A. W., and Sugiura, M. (2004)

Biosynthetic Ca^{2+}/Sr^{2+} exchange in the photosystem II oxygen-evolving enzyme of *Thermosynechococcus elongates*. *J. Biol. Chem. 279*, 22809−22819.
(48) Takahashi, R., Sugiura, M., and Noguchi, T. (2007) Water molecules coupled to the redox-active tyrosine Y_D in photosystem II as detected by FTIR spectroscopy. *Biochemistry 46*, 14245−14249.
(49) Frisch, M. J., Trucks, G. W., Schlegel, H. B., Scuseria, G. E., Robb, M. A., Cheeseman, J. R., Scalmani, G., Barone, V., Mennucci, B., Petersson, G. A., Nakatsuji, H., Caricato, M., Li, X., Hratchian, H. P., Izmaylov, A. F., Bloino, J., Zheng, G., Sonnenberg, J. L., Hada, M., Ehara, M., Toyota, K., Fukuda, R., Hasegawa, J., Ishida, M., Nakajima, T., Honda, Y., Kitao, O., Nakai, H., Vreven, T., Montgomery, J. A., Jr., Peralta, J. E., Ogliaro, F., Bearpark, M., Heyd, J. J., Brothers, E., Kudin, K. N., Staroverov, V. N., Kobayashi, R., Normand, J., Raghavachari, K., Rendell, A., Burant, J. C., Iyengar, S. S., Tomasi, J., Cossi, M., Rega, N., Millam, J. M., Klene, M., Knox, J. E., Cross, J. B., Bakken, V., Adamo, C., Jaramillo, J., Gomperts, R., Stratmann, R. E., Yazyev, O., Austin, A. J., Cammi, R., Pomelli, C., Ochterski, J. W., Martin, R. L., Morokuma, K., Zakrzewski, V. G., Voth, G. A., Salvador, P., Dannenberg, J. J., Dapprich, S., Daniels, A. D., Farkas, O., Foresman, J. B., Ortiz, J. V., Cioslowski, J., and Fox, D. J. (2009) *Gaussian 09*, revision C.01, Gaussian, Inc., Wallingford, CT.
(50) Becke, A. D. (1993) Density-functional thermochemistry. III. The role of exact exchange. *J. Chem. Phys. 98*, 5648−5652.
(51) Lee, C., Yang, W., and Parr, R. G. (1988) Development of the Colle-Salvetti correlation-energy formula into a functional of the electron density. *Phys. Rev. B 37*, 785−789.
(52) Vreven, T., Byun, K. S., Komaromi, I., Dapprich, S., Montgomery, J. A., Morokuma, K., and Frisch, M. J. (2006) Combining quantum mechanics methods with molecular mechanics methods in ONIOM. *J. Chem. Theory Comput. 2*, 815−826.
(53) Luber, S., Rivalta, I., Umena, Y., Kawakami, K., Shen, J. R., Kamiya, N., Brudvig, G. W., and Batista, V. S. (2011) S_1-state model of the O_2-evolving complex of photosystem II. *Biochemistry 50*, 6308−6311.
(54) Hasegawa, K., Ono, T., and Noguchi, T. (2000) Vibrational spectra and ab initio DFT calculations of 4-methylimidazole and its different protonation forms: Infrared and Raman markers of the protonation state of a histidine side chain. *J. Phys. Chem. B 104*, 4253−4265.
(55) Hienerwadel, R., Boussac, A., Breton, J., Diner, B. A., and Berthomieu, C. (1997) Fourier transform infrared difference spectroscopy of photosystem II tyrosine D using site-directed mutagenesis and specific isotope labeling. *Biochemistry 36*, 14712−14723.
(56) Noguchi, T., Inoue, Y., and Tang, X.-S. (1997) Structural coupling between the oxygen-evolving Mn cluster and a tyrosine residue in photosystem II as revealed by Fourier transform infrared spectroscopy. *Biochemistry 36*, 14705−14711.
(57) Takahashi, R., and Noguchi, T. (2007) Criteria for determining the hydrogen-bond structures of a tyrosine side chain by Fourier transform infrared spectroscopy: Density functional theory analyses of model hydrogen-bonded complexes of *p*-cresol. *J. Phys. Chem. B 111*, 13833−13844.
(58) Onidas, D., Stachnik, J. M., Brucker, S., Kratzig, S., and Gerwert, K. (2010) Histidine is involved in coupling proton uptake to electron transfer in photosynthetic proteins. *Eur. J. Cell Biol. 89*, 983−989.
(59) Noguchi, T., Inoue, Y., and Tang, X.-S. (1999) Structure of a histidine ligand in the photosynthetic oxygen-evolving complex as studied by light-induced Fourier transform infrared difference spectroscopy. *Biochemistry 38*, 10187−10195.
(60) Breton, J., and Nabedryk, E. (1998) Proton uptake upon quinone reduction in bacterial reaction centers: IR signature and possible participation of a highly polarizable hydrogen bond network. *Photosynth. Res. 55*, 301−307.
(61) Noguchi, T., Inoue, Y., and Tang, X. S. (1999) Hydrogen bonding interaction between the primary quinone acceptor Q_A and a histidine side chain in photosystem II as revealed by Fourier transform infrared spectroscopy. *Biochemistry 38*, 399−403.
(62) Suzuki, H., Nagasaka, M., Sugiura, M., and Noguchi, T. (2005) Fourier transform infrared spectrum of the secondary quinone electron acceptor Q_B in photosystem II. *Biochemistry 44*, 11323−11328.
(63) Iwata, T., Paddock, M. L., Okamura, M. Y., and Kandori, H. (2009) Identification of FTIR bands due to internal water molecules around the quinone binding sites in the reaction center from *Rhodobacter sphaeroides*. *Biochemistry 48*, 1220−1229.
(64) Hays, A. M. A., Vassiliev, I. R., Golbeck, J. H., and Debus, R. J. (1999) Role of D1-His190 in the proton-coupled oxidation of tyrosine Y_Z in manganese-depleted photosystem II. *Biochemistry 38*, 11851−11865.
(65) Meot-Ner, M. (2005) The ionic hydrogen bond. *Chem. Rev. 105*, 213−284.
(66) Gilli, P., Pretto, L., Bertolasi, V., and Gilli, G. (2009) Predicting hydrogen-bond strengths from acid-base molecular properties. The pK_a slide rule: Toward the solution of a long-lasting problem. *Acc. Chem. Res. 42*, 33−44.
(67) Freindorf, M., Kraka, E., and Cremer, D. (2012) A comprehensive analysis of hydrogen bond interactions based on local vibrational modes. *Int. J. Quantum Chem. 112*, 3174−3187.
(68) O'Malley, P. J. (2000) Density functional studies of phenoxyl-Na^+ ion complexes: Implications for tyrosyl free radical interactions in vitro. *Chem. Phys. Lett. 325*, 69−72.
(69) O'Malley, P. J. (2002) Density functional calculations modelling tyrosine oxidation in oxygenic photosynthetic electron transfer. *Biochim. Biophys. Acta 1553*, 212−217.
(70) Janosche, R., Weideman, E. G., Pfeiffer, H., and Zundel, G. (1972) Extremely high polarizability of hydrogen-bonds. *J. Am. Chem. Soc. 94*, 2387−2396.
(71) Zundel, G. (1988) Proton transfer in and proton polarizability of hydrogen bonds: IR and theoretical studies regarding mechanisms in biological systems. *J. Mol. Struct. 177*, 43−68.
(72) Zundel, G. (2000) Hydrogen bonds with large proton polarizability and proton transfer processes in electrochemistry and biology. *Adv. Chem. Phys. 111*, 1−217.
(73) Wang, J., and El-Sayed, M. A. (2001) Time-resolved Fourier transform infrared spectroscopy of the polarizable proton continua and the proton pump mechanism of bacteriorhodopsin. *Biophys. J. 80*, 961−971.
(74) Freier, E., Wolf, S., and Gerwert, K. (2011) Proton transfer via a transient linear water-molecule chain in a membrane protein. *Proc. Natl. Acad. Sci. U.S.A. 108*, 11435−11439.
(75) Noguchi, T., Suzuki, H., Tsuno, M., Sugiura, M., and Kato, C. (2012) Time-resolved infrared detection of the proton and protein dynamics during photosynthetic oxygen evolution. *Biochemistry 51*, 3205−3214.
(76) Noguchi, T., and Sugiura, M. (2002) FTIR detection of water reactions during the flash-induced S-state cycle of the photosynthetic water oxidizing complex. *Biochemistry 41*, 15706−15712.
(77) Polander, B. C., and Barry, B. A. (2013) Detection of an intermediary, protonated water cluster in photosynthetic oxygen evolution. *Proc. Natl. Acad. Sci. U.S.A. 110*, 10634−10639.
(78) Noguchi, T., and Sugiura, M. (2003) Analysis of flash-induced FTIR difference spectra of the S-state cycle in the photosynthetic water-oxidizing complex by uniform ^{15}N and ^{13}C isotope labeling. *Biochemistry 42*, 6035−6042.
(79) Tsuno, M., Suzuki, H., Kondo, T., Mino, H., and Noguchi, T. (2011) Interaction and inhibitory effect of ammonium cation in the oxygen evolving center of photosystem II. *Biochemistry 50*, 2506−2514.
(80) Suzuki, H., Taguchi, Y., Sugiura, M., Boussac, A., and Noguchi, T. (2006) Structural perturbation of the carboxylate ligands to the manganese cluster upon Ca^{2+}/Sr^{2+} exchange in the S-state cycle of photosynthetic oxygen evolution as studied by flash-induced FTIR difference spectroscopy. *Biochemistry 45*, 13454−13464.
(81) Nugent, J. H. A., Ball, R. J., and Evans, M. C. W. (2004) Photosynthetic water oxidation: The role of tyrosine radicals. *Biochim. Biophys. Acta 1655*, 217−221.

(82) Siegbahn, P. E. M., and Blomberg, M. R. A. (2010) Quantum chemical studies of proton-coupled electron transfer in metalloenzymes. *Chem. Rev. 110*, 7040−7061.
(83) Ishikita, H., Saenger, W., Loll, B., Biesiadka, J., and Knapp, E. W. (2006) Energetics of a possible proton exit pathway for water oxidation in photosystem II. *Biochemistry 45*, 2063−2071.
(84) Bao, H., Dilbeck, P. L., and Burnap, R. L. (2013) Proton transport facilitating water-oxidation: The role of second sphere ligands surrounding the catalytic metal cluster. *Photosynth. Res. 116*, 215−229.
(85) Pokhrel, R., McConnell, I. L., and Brudvig, G. W. (2011) Chloride regulation of enzyme turnover: Application to the role of chloride in photosystem II. *Biochemistry 50*, 2725−2734.
(86) Suzuki, H., Yu, J., Kobayashi, T., Nakanishi, H., Nixon, P., and Noguchi, T. (2013) Functional roles of D2-Lys317 and the interacting chloride ion in the water oxidation reaction of photosystem II as revealed by Fourier transform infrared analysis. *Biochemistry 52*, 4748−4757.
(87) Pokhrel, R., Service, R. J., Debus, R. J., and Brudvig, G. W. (2013) Mutation of lysine 317 in the D2 subunit of photosystem II alters chloride binding and proton transport. *Biochemistry 52*, 4758−4773.
(88) Clausen, J., Debus, R. J., and Junge, W. (2004) Time-resolved oxygen production by PSII: Chasing chemical intermediates. *Biochim. Biophys. Acta 1655*, 184−194.
(89) Hundelt, M., Hays, A. M., Debus, R. J., and Junge, W. (1998) Oxygenic photosystem II: The mutation D1-D61N in *Synechocystis* sp. PCC 6803 retards S-state transitions without affecting electron transfer from Y_Z to $P680^+$. *Biochemistry 37*, 14450−14456.
(90) Dilbeck, P. L., Hwang, H. J., Zaharieva, I., Gerencser, L., Dau, H., and Burnap, R. L. (2012) The D1-D61N mutation in *Synechocystis* sp. PCC 6803 allows the observation of pH-sensitive intermediates in the formation and release of O_2 from photosystem II. *Biochemistry 51*, 1079−1091.
(91) de Grotthuss, C. J. T. (1806) Sur la décomposition de l'eau et des corps qu'elle tient en dissolution à l'aide de l'électricité galvanique. *Ann. Chim. 58*, 54−73.
(92) Cukierman, S. (2006) Et tu Grotthuss! and other unfinished stories. *Biochim. Biophys. Acta 1757*, 876−885.
(93) Haumann, M., Liebisch, P., Müller, C., Barra, M., Grabolle, M., and Dau, H. (2005) Photosynthetic O_2 formation tracked by time-resolved X-ray experiments. *Science 310*, 1019−1021.